A High Avidity Biosensor Reveals PI(3,4)P_2 is Predominantly a Class I PI3K Signaling Product

Brady D. Goulden[1], Jonathan Pacheco[1], Allyson Dull[1], James P. Zewe[1], Alexander Deiters[2] and Gerald R. V. Hammond[1]

[1]Department of Cell Biology, University of Pittsburgh School of Medicine and
[2]Department of Chemistry, University of Pittsburgh, Pittsburgh, PA, USA

Running title: A High Avidity Biosensor for PI(3,4)P_2

Keywords: PtdIns(3,4)P_2; inositol lipid; phosphoinositides.

Abstract

Class I PI 3-kinase (PI3K) signaling is central to animal growth and metabolism, and disruption of this pathway occurs frequently in cancer and diabetes. However, the specific spatial/temporal dynamics and signaling roles of its minor lipid messenger, phosphatidylinositol (3,4)-bisphosphate [$PI(3,4)P_2$], are not well understood. This owes principally to a lack of tools to study this scarce lipid. Here, we developed a high sensitivity genetically encoded biosensor for $PI(3,4)P_2$, demonstrating high selectivity and specificity of the sensor for the lipid. We show that despite clear evidence for class II PI3K in $PI(3,4)P_2$-driven function, the overwhelming majority of the lipid accumulates through degradation of class I PI3K-produced PIP_3. However, we show that $PI(3,4)P_2$ is also subject to hydrolysis by the tumor suppressor lipid phosphatase PTEN. Collectively, our results show that $PI(3,4)P_2$ is potentially an important driver of class I PI3K-driven signaling, and provides powerful new tools to begin to resolve the biological functions of this lipid downstream of class I and II PI3K.

Introduction

Class I phosphoinositide 3-OH kinase (PI3K) signaling is central to the control of growth and metabolism in animals (Vanhaesebroeck et al., 2012). Overactivation of this pathway is the most common event in cancer (Fruman et al., 2017), yet given its major role in insulin signaling, inhibition of the pathway triggers insulin resistance and type 2 diabetes (Hopkins et al., 2018). Therefore, the ability to selectively manipulate PI3K signaling could have tremendous therapeutic benefit. Efforts to accomplish this goal are a major focus of the biomedical enterprise (Fruman et al., 2017)

At the molecular level, PI3K signaling involves the generation of the plasma membrane (PM) second messenger lipids phosphatidylinositol 3,4,5-trisphosphate (PIP_3) and phosphatidylinositol 3,4-bisphosphate [$PI(3,4)P_2$] that activate downstream effector proteins like the serine/threonine kinase Akt. PIP_3 is the major lipid produced, and most functions of the pathway are attributable to it (Vanhaesebroeck et al., 2012). $PI(3,4)P_2$ has instead been viewed as either a degradation product (Ishihara et al., 1999), or as an alternative activator of the pathway (Ebner et al., 2017). However, selective functions for $PI(3,4)P_2$ have recently been described that are independent of PIP_3 (Li and Marshall, 2015). These include the formation of lamellipodia and invadopodia (Krause et al., 2004; Bae et al., 2010; Oikawa et al., 2008; Sharma et al., 2013), along with clathrin-mediated and clathrin-independent endocytosis (Posor et al., 2013; Boucrot et al., 2015) In each case, these functions could conceivably be driven by, or occur independently of, class I PI3K signaling.

Synthesis of $PI(3,4)P_2$ can proceed via three routes: In the first, class I PI3K directly generates $PI(3,4)P_2$ and PIP_3 by 3-OH phosphorylation of the respective PM phosphoinositides PI4P and $PI(4,5)P_2$ (Carpenter et al., 1990). Subsequently, the observation that $PI(3,4)P_2$ synthesis lags behind PIP_3 in stimulated cells (Stephens et al., 1991; Jackson et al., 1992; Hawkins et al., 1992), coupled with the discovery of the PIP_3-specific 5-phopshatase enzymes SHIP1 and SHIP2 (Damen et al., 1996; Pesesse et al., 1997), led to the proposal of a second route: $PI(3,4)P_2$ production by removal of the 5-OH phosphate from PIP_3. More recently, a third route has been established, again invoking direct phosphorylation of PI4P, this time by class II PI3K enzymes (Domin et al., 1997; Posor et al., 2013). However, the relative contributions of these

pathways, and how they couple to disparate PI(3,4)P_2-dependent cellular functions, remains unclear (Li and Marshall, 2015).

Resolving how the spatial/temporal dynamics of PI(3,4)P_2 signaling couples to different biological functions requires approaches to identify the lipid in intact, living cells. Isolated lipid binding domains fused to fluorescent reporters often make highly selective genetically encoded biosensors for this purpose (Wills et al., 2018). The pleckstrin homology (PH) domain on the C-terminus of TAPP1 (TAndem Ph-domain containing Protein 1) exhibits specific binding to PI(3,4)P_2 in the test tube (Thomas et al., 2001; Dowler et al., 2000). As a result, several studies have employed fluorescent protein conjugates of this domain to track PI(3,4)P_2 signaling, though the domain fails to detect resting levels or the limited accumulation of the lipid in response to stimuli such as insulin-like growth factor (Kimber et al., 2002; Marshall et al., 2002; Oikawa et al., 2008; Posor et al., 2013).

Herein, we developed a higher-avidity tandem trimer of PH-TAPP1. We show PI(3,4)P_2 generation is sufficient to recruit the probe, which is exquisitely selective for the lipid over other phosphoinositides. We then demonstrate that the class I PI3K pathway, acting via PIP_3 synthesis, dominates PI(3,4)P_2 accumulation in cells. Our data also support the recently proposed direct degradation of both PI(3,4)P_2 and PIP_3 by the lipid phosphatase and tumor suppressor PTEN (Malek et al., 2017). Collectively, our data show that the class I PI3K pathway is the most potent driver of PI(3,4)P_2-dependent signaling.

Results

cPH probes selectively bind plasma membrane PI(3,4)P_2

The TAPP1 protein (encoded by the *PLEKHA1* gene) contain both N- and C-terminal PH domains (figure 1A), the latter of which selectively binds PI(3,4)P_2 (Dowler et al., 2000). Previous studies using the isolated TAPP1 C-terminal PH domain (cPH) as a lipid biosensor found no detectable translocation in response to stimuli that induce modest PI(3,4)P_2 accumulation (Kimber et al., 2002). To improve avidity, tandem dimers of TAPP1 fragments containing the cPH domain have been employed (Oikawa et al., 2008; Posor et al., 2013; He et al., 2017). However, these constructs are based on a fragment including the entire C-terminus (Furutani et al., 2006), which carries binding sites for other proteins in its tail, and have been shown to induce dominant negative effects (Kimber et al., 2002; Hogan et al., 2004; Thalappilly et al., 2008; Li and Marshall, 2015). Therefore, we built tandem dimers and trimers of the isolated cPH domain (residues 169-329 in human TAPP1) as previously defined (Marshall et al., 2002), and included a nuclear export sequence (figure 1A).

Expression of EGFP-tagged cPH monomers, dimers or trimers in COS-7 cells maintained in 10% serum exhibit a predominantly cytosolic localization of the probe when viewed by confocal microscopy (figure 1B). However, comparison with another cytosolic protein (infra-red fluorescent protein, iRFP) revealed enrichment of cPHx2 and cPHx3 at the cell periphery; normalization of the two signals followed by subtracting the iRFP signal from that of EGFP (see Materials and Methods) showed striking cPHx2/3 peripheral localization (figure 1B). This signal was abolished by a PM-targeted INPP4B phosphatase that specifically degrades PI(3,4)P_2 (Gewinner et al., 2009), though not by a catalytically inactive mutant (figure 1B). Quantification of the difference between EGFP and iRFP signals (figure 1C with Kruskal-Wallis statistic 152.5; $p < 10^{-4}$) yielded significantly increasing signal from cPHx1 to x3; INPP4B-CAAX significantly reduced cPHx3 signal ($p < 10^{-4}$ in each case, Dunn's multiple comparison test), whereas the C842A inactive mutant did not ($p > 0.99$). Therefore, cPHx2 and cPHx3 could detect PI(3,4)P_2 at the plasma membrane of living cells in the presence of serum.

A potential caveat to using tandem arrays of lipid binding domains is that the resulting probe may cluster lipids and exhibit aberrant localization or mobility in the membrane. To determine whether this was the case, we performed single molecule imaging of cPHx1, x2 and x3 mobility

in the plasma membrane by tagging with photoactivatable mCherry (PAmCherry). As shown in figure 1D, full activation of the probe with violet light led to uniform labelling of the plasma membrane in total internal reflection fluorescence microscopy (TIRFM), whereas low activation intensities allowed us to image single molecule trajectories (Manley et al., 2008). Analysis of the mean square displacement of these trajectories over time revealed free Brownian motion of all three probes (figure 1E). cPHx1, x2 and x3 diffused with an apparent diffusion coefficient of ~0.3 $\mu m^2/s$ (figure 1F) and did not substantially differ ($F = 0.71$, $p = 0.50$, one-way ANOVA), and all exhibited a relative deviation ratio close to 1 (figure 1G), meaning there was no substantial difference in actual displacement relative to that predicted by free Brownian diffusion (Fujiwara et al., 2016). Therefore, the tandem array of domains did not slow the probe's mobility in the membrane.

The lifetime distribution of the single molecules on the membrane followed a single exponential decay with a characteristic "off rate" constant (k_{off}) that increased linearly with laser power due to increased photobleaching (figure 1H). Extrapolation of this off rate to the intercept at zero illumination power allowed us to estimate the true off rate of the probes. cPHx1 has a lifetime on the membrane of approximately 90 ms (off rate $= 11\ s^{-1}$), whereas cPHx2 and cPHx3 both showed lifetimes of approximately 140 ms. This change in dissociation rate of the tandem arrays was comparatively modest, and certainly not multiplicative as would be expected from multi-ligand binding. This implies that, for the majority of probe molecules at steady state, the PH domains are not all occupied by lipid, most likely because of the low abundance of $PI(3,4)P_2$. The enhanced PM binding observed in figure 1C likely stems from transient dual or triple occupancy of the PH domains slowing the overall off-rate of the population (and perhaps enhancing the on rate for cPHx3 vs cPHx2).

A potential limitation of biosensors is that when bound to lipid, they will protect the lipid from consumption by enzymes and occlude interaction with endogenous effector proteins, both of which may be needed for local enrichment of the lipid. Therefore, free diffusion of the probe:lipid complex can disrupt local enrichment rather than reporting on it. From the relationship $r = (2D/k_{off})^{0.5}$ (Teruel and Meyer, 2000), the distance, r, that cPHx3 typically diffuses while attached to lipid can be estimated as ~290 nm, not much larger than the diffraction limit. This implies there will be a limited propensity of the probes' free diffusion to "smear out" local enrichment of $PI(3,4)P_2$ molecules that are detectable with diffraction-limited optical imaging.

To determine if PM localization of cPH probes is sensitive to acute depletion of $PI(3,4)P_2$, we utilized chemically-induced dimerization between FK506 binding protein 12 (FKBP) and the FKBP12 Rapamycin Binding (FRB) domain of mTor (Belshaw et al., 1996) to recruit INPP4B to the PM (figure 1I). Rapamycin-induced dimerization and thus INPP4B recruitment led to depletion of PM-associated cPH signal in TIRFM (figure 1J, two-way ANOVA of area under the curve [AUC] before and after rapamycin addition, $F(1, 200) = 314.5$, $p < 10^{-4}$; $p < 10^{-4}$ for cPHx1, x2 and x3, Sidak's multiple comparisons test). The depletion was progressively greater for cPHx3 > cPHx2 > cPHx1 (comparing AUC, $F = 75.64$; $p < 10^{-4}$; cPHx2 vs cPHx3, $p = 0.02$; cPHx1 vs cPHx2, $p < 10^{-4}$), reflecting the increased avidity of the tandem probes for PM $PI(3,4)P_2$. On the other hand, probes for other inositol lipids, including PI4P (P4Mx1), $PI(4,5)P_2$ (PH-PLCD1), PIP_3 (PH-ARNO^{2G}x2) or $PI(3,4)P_2$/PIP_3 (PH-AKT) did not show a significant change (Hammond et al., 2014; Várnai and Balla, 1998; Venkateswarlu et al., 1998; Watton and Downward, 1999). Notably, when the data were normalized to emphasize the kinetics of the change, no difference between the rates of cPHx1, x2 or x3 dissociation after INPP4B recruitment were observed (figure 1J, right; Kruskal-Wallis statistic = 1.19, $p = 0.55$), indicating that the higher avidity tandem probes did not effectively sequester lipid from the INPP4B enzyme. Furthermore, recruitment of inactive INPP4B mutant C842A did not lead to substantial depletion of the cPH probes from the PM (figure 1K).

Given the much higher avidity of cPHx3 and x2 for the PM, we wanted to rule out a weak interaction with other lipids that might synergize to influence PM targeting by these probes. To this end, we used chemically induced dimerization again, this time using the INPP5E phosphatase domain (figure 1L), since this domain is active against $PI(4,5)P_2$ and PIP_3, generating PI4P and $PI(3,4)P_2$, respectively (Asano et al., 1999; Kong et al., 2000). INPP5E recruitment did not displace PI4P-binding P4Mx1 or any of the cPH probes from the PM, though it did displace probes that bound to PIP_3 or $PI(4,5)P_2$ (figure 1M). Therefore, these two inositol lipids do not influence the PM-association of cPH probes.

Together, these results allowed us to conclude that (i) the cPHx3 probe derived from TAPP1 exhibits significantly greater localization than previously used single and tandem dimer versions, (ii) the tandem trimer configuration does not disrupt free diffusion in the plane of the membrane nor sequester $PI(3,4)P_2$ to an extent that prevents INPP4B access and (iii) exhibits localization that depends solely on the phosphoinositide $PI(3,4)P_2$. These are crucial criteria in the definition

of a reliable genetically encoded lipid biosensor. However, there is another critical criterion that must be met, which we tested next.

PI(3,4)P_2 is sufficient for cPHx3 cellular localization

We have argued that a crucial but often ignored criterion for a high-fidelity lipid biosensor is a sole requirement of the lipid to drive biosensor localization (Wills et al., 2018). A convenient way to test this criterion is to induce ectopic synthesis of the lipid elsewhere in the cell and test whether this is sufficient to recruit the biosensor (Hammond et al., 2014). To this end, we turned to the *Legionella* effector protein LepB, the N-terminus of which possesses PI3P 4-OH kinase activity, thus generating PI(3,4)P_2 via a non-canonical pathway not utilized by mammalian cells (Dong et al., 2016). We found that expression of LepB led to substantial PI3P depletion from cells, and consequent swelling of the endosomal compartment that depends on this lipid for function (B.D.G and G.R.V.H., unpublished observations). Therefore, to induce acute LepB activity, we turned to an optogenetic approach that utilizes genetic code expansion to incorporate an unnatural, caged amino acid into the protein (Luo et al., 2014; Liu et al., 2017; Courtney and Deiters, 2018).

This system relies on mutating the target protein at the desired codon to the infrequently used amber stop codon (UAG). The mutant gene is then transfected into cells along with plasmids encoding an engineered pyrrolysyl-tRNA synthetase/tRNA pair and the caged amino acid is added to the media. Here, a hydroxycoumarin-caged lysine (HCK) is transacylated onto the tRNA and thence ribosomally incorporated into the mutated gene in response to the UAG codon. In the context of LepB, the bulky hydroxycoumarin group incorporated onto lysine 39 blocks the active site (Dong et al., 2016). However, illumination of cells expressing this system with 405 nm light causes photolysis of the coumarin group, liberating the lysine residue, and generating wild-type, active LepB (figure 2A). This provides precise and acute spatiotemporal control over LepB function in live human cells.

Optogenetic activation of LepB in cells expressing cPHx3 caused synthesis of PI(3,4)P_2 on endosomes and striking recruitment of the cPHx3 probe (figure 2B). This optogenetic activation was only observed in cells grown in the presence of exogenous HCK, and depended on co-transfection with the LepB^{K39UAG}, ruling out off-target effects on endogenous UAG-containing genes or of light-exposure alone. Similarly, we observed clear translocation of PH-AKT to

endosomes, which is expected given this PH domain's binding to both PIP_3 and $PI(3,4)P_2$ (Ebner et al., 2017). However, no recruitment of the PIP_3-specific PH-$ARNO^{2G}$x2 was observed (Venkateswarlu et al., 1998; Manna et al., 2007), demonstrating that there was no further phosphorylation of the lipid at the 5-OH. Finally, we observed some depletion of the PI3P biosensor FYVE-EEA1 (Wills et al., 2018), though the biosensor remained mostly endosome-bound, indicating a small fraction of total PI3P was converted to $PI(3,4)P_2$ over the time course of these experiments (figure 2B).

Collectively, these results demonstrate that generation of $PI(3,4)P_2$ in a cellular membrane is indeed sufficient to recruit cPHx3, which given its extensive *in vitro* selectivity (Dowler et al., 2000; Thomas et al., 2001), now passes all the key criteria that define a high-fidelity, genetically encoded biosensor for $PI(3,4)P_2$ (Wills et al., 2018). The fidelity of the probe established, we next turned our attention to deploying this tool to answer some central questions about the lipid's metabolism and function.

Dominance of Class I PI3K in $PI(3,4)P_2$ synthesis

The canonical view of $PI(3,4)P_2$ synthesis induced by Class I PI3K signaling is that PI3K generates PIP_3, which is then dephosphorylated at the 5-OH position by inositol polyphosphatase 5-phosphatase (INPP5) family members SHIP1 or SHIP2 (Vanhaesebroeck et al., 2012). Both enzymes are activated by tyrosine phosphorylation cascades initiated by the activated receptor tyrosine kinase. The extent of $PI(3,4)P_2$ accumulation varies depending on receptor activation, with insulin or insulin-like growth factor reported to generate only modest amounts of the lipid (Jackson et al., 1992; Guilherme et al., 1996), which have not been detected with a single cPH probe (Kimber et al., 2002).

We tested the capacity of cPHx3 to detect insulin-induced $PI(3,4)P_2$ production in HeLa cells (Figure 3A). To unambiguously detect PIP_3 in the same cells, we employed a tandem dimer of the PH domain from ARNO, specifically selecting the 2G splice variant with high PIP_3 affinity (Cronin et al., 2004) and introducing the I303E mutation that prevents PH domain interaction with Arl GTPases (Hofmann et al., 2007). We selected this domain since it exhibits clear discrimination for PIP_3 over $PI(3,4)P_2$ (Manna et al., 2007). Insulin stimulation of HeLa cells generated a robust, transient increase in PIP_3 biosensor at the PM, with a lagging, yet more sustained appearance of the $PI(3,4)P_2$ biosensor (figure 3B, C) – a clear recapitulation of the

original biochemical measurements of PI3K product generation (Stephens et al., 1991; Jackson et al., 1992; Hawkins et al., 1992), apparently supporting the canonical view.

As an alternative mechanism to activate Class I PI3K, we turned to chemically induced dimerization to recruit the inter-Src Homology 2 (iSH2) domain from the p85 regulatory subunit of PI3K (figure 3A). This system recruits endogenous PI3K p110 catalytic subunits to the membrane, inducing PIP_3 synthesis (Suh et al., 2006). However, in this situation, tyrosine kinase-mediated activation of SHIP phosphatases is not expected. Nevertheless, iSH2 recruitment to the PM of COS-7 cells induced rapid PIP_3 synthesis and the same, lagging $PI(3,4)P_2$ accumulation (figure 3D). We therefore speculated that, in this context at least, $PI(3,4)P_2$ accumulation might be driven by direct phosphorylation of PI4P by p110, given that the enzyme is known to perform this reaction in a test tube (Carpenter et al., 1990).

To test this speculation, we devised an experiment wherein the INPP5E enzyme would be co-recruited to the PM in conjunction with iSH2. Since INPP5E will deplete both $PI(4,5)P_2$ and PIP_3, accumulation of PIP_3 should be prevented (figure 3E). PIP_3 will be degraded into $PI(3,4)P_2$ – but synthesis of $PI(3,4)P_2$ will only be sustained if the p110 enzymes indeed directly converts PI4P into $PI(3,4)P_2$. Compared with controls using a catalytically impaired INPP5E D556A mutant, INPP5E completely blocked the accumulation of the PIP_3 biosensor at the PM after co-recruitment (figure 3F). However, cPHx3 initially recruited to the PM at a similar rate to control, though its synthesis was rapidly cut off when INPP5E was co-recruited (figure 3G). Therefore, $PI(3,4)P_2$ synthesis cannot be sustained in the absence of PIP_3 generation, even under conditions where SHIP phosphatases are not predicted to become activated. Presumably, the PIP_3 5-phosphatase activity responsible either comes from basal SHIP activity through interaction of its C2 domain with acidic PM lipids (Ong et al., 2007; Coq et al., 2017), or else from other INPP5 family members, which are all competent at converting PIP_3 to $PI(3,4)P_2$ (Trésaugues et al., 2014). Identification of the enzymes responsible will be a key question for future work.

Thus far, these experiments addressed the pool of $PI(3,4)P_2$ generated downstream of Class I PI3K signaling. However, activity of class II PI3K have been shown to function in a more constitutive capacity (Posor et al., 2013; Marat et al., 2017). We therefore wanted to identify the source of $PI(3,4)P_2$ that we observed at the PM in growing cells (figure 1). To this end, we employed the potent and Class I PI3K-selective inhibitor GDC-0941 (Kong et al., 2010) at 250

nM to distinguish Class I and Class II activities (figure 3H). After inhibitor treatment for 20 min, cells were subject to chemically-induced dimerization to recruit a co-expressed FKBP-INPP4B to the PM (figure 3I), the goal being to degrade any remaining PI(3,4)P_2. As shown in figure 3I, GDC treatment led to the depletion of almost the entire pool of PM-associated PI(3,4)P_2 from cells grown in serum. We cannot rule out that the small additional decrease induced in the 5 min after rapamycin addition is not an addition artifact (figure 3I); area under the curve measurements for post rapamycin treatment vs. the 5 min period preceding it do not show a significant change ($p = 0.43$, Sidak's multiple comparisons test) as compared to the change following DMSO treatment ($p < 10^{-4}$, Sidak's multiple comparison test after 2-way repeated-measures test, $F = 61.9$, $p < 10^{-4}$). However, the data do clearly indicate that the overwhelming majority of PI(3,4)P_2 present in the PM of cells is generated by the class I PI3K pathway.

Direct Hydrolysis of PI(3,4)P_2 by PTEN

So far, our data support a canonical view of Class I PI3K signaling, which is dominated by conversion of PI(4,5)P_2 to PIP_3, followed by degradation back to PI(4,5)P_2 by PTEN or conversion to PI(3,4)P_2 via INPP5 enzymes, most prominently SHIP1 and SHIP2 (Vanhaesebroeck et al., 2012; Fruman et al., 2017). PTEN and INPP5 thus represent a bifurcation of the pathway: in the former case, towards a simple inactivation; in the latter, the conversion to a modified but still active signaling state (Li and Marshall, 2015). PI(3,4)P_2 is ultimately degraded to PI3P by INPP4A/B, a process intimately linked to endocytosis (Shin et al., 2005). However, it has been perplexing that the accumulation of PI(3,4)P_2 seen after PI3K activation does not lead to a detectable increase in PI3P levels (Jackson et al., 1992; Stephens et al., 1991), implying an alternative route of degradation. Recently, Malek and colleagues have proposed that PTEN in fact directly converts PI(3,4)P_2 to PI4P, terminating this signaling as well (Malek et al., 2017). The evidence was based on the requirement for PTEN knockout for EGF-stimulated PI(3,4)P_2 accumulation, in addition to showing that a PI(3,4)P_2 3-phosphatase activity in MCF10 cell cytosol was lost in PTEN nulls. However, direct evidence for hydrolysis of PI(3,4)P_2 in intact, living cells is still lacking.

The principle reason for the ongoing ambiguity over cellular activity of PTEN against PI(3,4)P_2 has been the ambiguity when interpreting changes in lipid levels in cells. When PTEN loss induces PI(3,4)P_2 accumulation, this can be explained by failure of PTEN to degrade PI(3,4)P_2 directly – or alternatively, due to impaired PIP_3 degradation, leaving more substrate available for

the INPP5 enzymes (figure 4A). Careful mathematical modeling suggested the latter explanation did not explain the accumulation in MCF10 cells (Malek et al., 2017). Nonetheless, the evidence is indirect. We therefore devised an experiment utilizing the LepB PI3P 4-OH kinase. Since we showed that this enzyme generates an endosomal pool of PI(3,4)P_2 devoid of PIP_3 (figure 2), activity of PTEN leading to depletion of PI(3,4)P_2 can be unambiguously assigned to direct hydrolysis of the lipid in this context (figure 4B).

Indeed, use of chemically-induced dimerization of FKBP-PTEN to FRB-LAMP1-positive endosomes/lysosomes caused a rapid depletion of endosomal PI(3,4)P_2 detected with cPHx3 in LepB-expressing COS-7 cells (figure 4C). That this was truly PI(3,4)P_2 to PI4P conversion induced by PTEN was further evidenced by a clear accumulation of PI4P on these membranes (figure 4D). Therefore, our data provide a direct demonstration of PI(3,4)P_2 hydrolysis by PTEN in intact, living cells – and confirms the novel role of this enzyme in terminating PI(3,4)P_2 signaling in addition to signals driven by PIP_3 (Malek et al., 2017).

Discussion

In this study, we report a high avidity probe for PI(3,4)P_2, cPHx3-TAPP1, which satisfies three crucial criteria for a genetically encoded lipid biosensor (Wills et al., 2018): (i) binding of the PH domain is exquisitely specific for PI(3,4)P_2 (Dowler et al., 2000; Thomas et al., 2001; Manna et al., 2007), (ii) PI(3,4)P_2 binding is absolutely necessary, and (iii) sufficient for localization in living cells (figures 1 and 3). [text] We use this high fidelity and high sensitivity probe to develop the first direct evidence for the canonical pathway of PI(3,4)P_2 synthesis by class I PI3K (i.e. by PIP_3 de-phosphorylation, figure 3), first proposed nearly three decades ago (Stephens et al., 1991; Hawkins et al., 1992). We also provide direct evidence for a much more recent proposition (Malek et al., 2017): that the tumor suppressor PTEN also terminates PI(3,4)P_2 signals in addition to those mediated by PIP_3 (figure 4). We also generated the first optogenetically activatable lipid kinase, LepB (figure 2).

How PI(3,4)P_2 signaling couples to different functions, and their relationship (or not) with the class I PI3K pathway, is still poorly understood (Li and Marshall, 2015; Hawkins and Stephens, 2016). This has largely been due to the difficulty in studying PI(3,4)P_2 in isolation from the other, more abundant phosphoinositides such as PI(4,5)P_2 and PIP_3. However, recent advances in mass spectrometry are allowing sensitive detection of this lipid (Malek et al., 2017; Bui et al., 2018). We anticipate that our tools and cPHx3 probe will complement these approaches and greatly accelerate research in this area.

For now, the clearest demonstration is that most PI(3,4)P_2 accumulating in cells is derived from INPP5 activity on class I PI3K-synthesized PIP_3. Without stimulation, resting levels of PI(3,4)P_2 are extremely low (Stephens et al., 1991; Hawkins et al., 1992), with immunocytochemical estimates suggesting that perhaps 40% of this is generated by the class II PI3K-C2α (Wang et al., 2018). The function of the greatly expanded class I PI3K-driven pool remains an ongoing question. Conversion of PIP_3 to PI(3,4)P_2 will terminate signals generated by PIP_3-selective effectors, maintain signals by more promiscuous effectors (like Akt), and initiate signaling by PI(3,4)P_2-selective effectors (Hawkins and Stephens, 2016). What is the purpose of this tiered lipid signaling system? A clue comes from perhaps the best characterized PI(3,4)P_2-selective effector protein: the TAPP proteins from which our probe is derived. Mice harboring point mutations in *Plekha1* and *Plekha2* that disrupt PI(3,4)P_2-binding of the TAPP1 and TAPP2 cPH domains exhibit augmented PI3K signaling through insulin and B-cell receptors (Gray and

Alessi, 2011; Landego et al., 2012), suggesting a major function of the lipid is in negative feedback of class I PI3K signaling. Interestingly, $PI(3,4)P_2$ is also implicated in endocytosis (Shin et al., 2005; Posor et al., 2013; Boucrot et al., 2015). Therefore, it could be possible that $PI(3,4)P_2$ downregulates PI3K signals by triggering internalization of activated receptors.

Such a model may reconcile conflicting data over the generation of $PI(3,4)P_2$ in clathrin mediated endocytosis. The class II PI3K-C2α was shown to generate a pool of $PI(3,4)P_2$ essential for constitutive endocytosis (Posor et al., 2013), whereas a co-incidence detector probe showed that the enzyme was dispensable for $PI(3,4)P_2$ accumulation at clathrin-coated structures (He et al., 2017). Although seemingly at odds, it is worth noting that careful quantitative modeling of lipid dynamics during formation of the clathrin bud found that just enough $PI(3,4)P_2$ is produced to recruit its SNX9 effector protein – meaning that the level of free lipid might be extremely low and invisible to even the most sensitive biosensor (Schöneberg et al., 2017). So why was $PI(3,4)P_2$ observed at clathrin structures at all (He et al., 2017)? We propose that the greatly expanded pool of class I PI3K synthesized $PI(3,4)P_2$ was being detected. Indeed, the cells in He et al were imaged in 5% serum, and most experiments were conducted in SUM159 cells, which have constitutive class I PI3K activation via the oncogenic 1047A mutation in p110α (Barnabas and Cohen, 2013). Intriguingly, $PI(3,4)P_2$ synthesis by class I PI3K activity was also found to be essential for clathrin-independent, fast endophilin mediated endocytosis (Boucrot et al., 2015). An attractive model is therefore that PI3K-C2α produces a minor pool of $PI(3,4)P_2$ that supports constitutive clathrin-mediated endocytosis, whereas greatly expanded pools downstream of Class I PI3K are required for accelerated clathrin-mediated and independent endocytosis after activation, whilst also sustaining Akt signaling.

A second major finding is that $PI(3,4)P_2$ is directly hydrolyzed by PTEN (Malek et al., 2017). This result is surprising, since meticulous work with purified protein found much poorer PTEN activity against $PI(3,4)P_2$ vs. PIP_3 (McConnachie et al., 2003). The discrepancy likely derives from the very different enzyme-substrate interactions in living cells; indeed, turnover numbers for PTEN in living cells are several orders of magnitude higher than in the test tube (McConnachie et al., 2003; Feng et al., 2014). It therefore seems likely that PTEN regulates $PI(3,4)P_2$ signaling in addition to PIP_3. Intriguingly, the recent observations that PTEN reduced signaling from forming clathrin-coated structures and slows their maturation is entirely consistent with the roles of both

class I and class II PI3K proposed in the previous paragraph (Rosselli-Murai et al., 2018). Finally, since PTEN's activity on PI(3,4)P_2 is the direct reversal of the PI4P conversion mediated by class II PI3K, and since PTEN has recently been found to localize to endosomal structures (Naguib et al., 2015), PTEN seems poised to regulate PI3K-C2β signaling from late endosomes/lysosomes too (Marat et al., 2017).

In summary, we have developed and validated a sensitive genetically encoded lipid biosensor for PI(3,4)P_2. We show this lipid accumulates in cells primarily in response to class I PI3K activity, via circuitous dephosphorylation of PIP_3. We also provide evidence for direct hydrolysis of PI(3,4)P_2 by PTEN. Collectively, these results provide fresh impetus to dissect the physiological and pathological signaling outcomes driven by PI(3,4)P_2, and provides a powerful new tool to aid in this endeavor.

Materials and Methods

Cell Culture and transfection

COS-7 (ATCC CRL-1651) and HeLa (ATCC CCL-2) cells were cultured in DMEM (low glucose; Life Technologies 10567022) supplemented with 10% heat-inactivated fetal bovine serum (Life Technologies 10438-034), 100 units/ml penicillin, 100 μg/ml streptomycin (Life Technologies 15140122) and 1:1000 chemically-defined lipid supplement (Life Technologies 11905031) at 37˚C in a humidified atmosphere with 5% CO_2. They were passaged twice per week by dissociation in TrpLE (Life Technologies 12604039) and diluting 1 in 5. For transfection, cells were seeded in 35 mm tissue culture dishes with 20 mm Number 1.5 cover glass apertures (CellVis) coated with 5 μg fibronectin (Life Technologies 33016-015). Between 1 and 24 hours post seeding, cells were transfected with 1 μg total plasmid DNA pre-complexed with 3 μg lipofectamine2000 (Life Technologies 11668019) in 200 μl Opti-MEM (Life Technologies 51985091) according to the manufacturer's instructions. Cells were imaged 18-26 h post-transfection. For unnatural amino acid incorporation, medium was supplemented with 250 μM hydroxycoumarin lysine in parallel with the transfection.

Plasmids

pPAmCherry-C1 (Addgene plasmid 31929) was a kind gift of Vladislav Verkhusha (Subach et al., 2009). EGFP (*Aequorea victoria* GFP with F64L and S65T mutations with human codon optimization), mCherry, *Rhodopseudomonas palustris* bacteriophytochrome BphP2-derived near-infrared fluorescent protein variant iRFP713 and *Entacmaea quadricolor* GFP-like protein eqFP578 variant pTagBFP2 were used in the Clontech pEGFP-C1 and N1 backbones as described previously (Zewe et al., 2018). TAPP1 cPH and LepB sequences were obtained as synthetic gblocks (IDT). All plasmids were verified by dideoxy sequencing. Constructs generated in this study are freely distributed through Addgene. Plasmids were constructed using standard restriction cloning or NEB HiFi assembly (New England Biolabs E5520S), or else obtained from the sources indicated below:

Plasmid	Backbone	Insert	Ref
NES-EGFP-cPHx1	pNES-EGFP-C1	*X.leavis* map2k1.L(32-44):EGFP:PLEKHA1(169-329)	This study
NES-EGFP-cPHx2	pNES-EGFP-C1	*X.leavis* map2k1.L(32-44):EGFP:PLEKHA1(169-329):GGSGGGSGG: PLEKHA1(169-329)	This study
NES-EGFP-cPHx3	pNES-EGFP-C1	*X.leavis* map2k1.L(32-44):EGFP:PLEKHA1(169-329):GGSGGGSGG: PLEKHA1(169-329): GGSGGGSGG: PLEKHA1(169-329)	This study
TagBFP2-CAAX	pTagBFP2-C1	TagBFP2:HRAS(172-189)	This study
TagBFP2-INPP4B-CAAX	pTagBFP2-C1	TagBFP2:INPP4B:HRAS(172-189)	This study
TagBFP2-INPP4B^{C842A}-CAAX	pPAmCherry-C1	TagBFP2:INPP4B(C842A):HRAS(172-189)	This study
NES-PAmCherry-cPHx1	pPAmCherry-C1	PAmCherry:PLEKHA1(169-329)	This study
NES-PAmCherry-cPHx2	pPAmCherry-C1	PAmCherry:PLEKHA1(169-329):GGSGGGSGG: PLEKHA1(169-329)	This study
NES-PAmCherry-cPHx3	pPAmCherry-C1	PAmCherry:PLEKHA1(169-329):GGSGGGSGG: PLEKHA1(169-329): GGSGGGSGG: PLEKHA1(169-329):	This study
NES-mCherry-cPHx3	pNES-mCherry-C1	mCherry:PLEKHA1(169-329):GGSGGGSGG: PLEKHA1(169-329): GGSGGGSGG: PLEKHA1(169-329):	This study
pNES-iRFP-C1	piRFP-C1	X.leavis map2k1.L(32-44):iRFP	This study
Lyn$_{11}$-FRB-iRFP	piRFP-N1	*LYN*(1-11):*MTOR*(2021-2113):iRFP	(Hammond et al., 2014)
LAMP1-FRB-iRFP	piRFP-N1	*LAMP1*:*MTOR*(2021-2113):iRFP	This study
mCherry-FKBP-INPP5E	pmCherry-C1	mCherry:*FKBP1A*(3-108):[GGSA]$_4$GG:INPP5E(214-644)	(Hammond et al., 2014)
mCherry-FKBP-INPP5E^{D556A}	pmCherry-C1	mCherry:*FKBP1A*(3-108):[GGSA]$_4$GG:INPP5E(214-644)	(Hammond et al., 2014)
mCherry-FKBP-INPP4B	pmCherry-C1	mCherry:*FKBP1A*(3-108):[GGSA]$_4$GG:INPP4B	This study
mCherry-FKBP-INPP4B^{C842A}	pmCherry-C1	mCherry:*FKBP1A*(3-108):[GGSA]$_4$GG:INPP4B(C842A)	This study
mCherry-FKBP-PTEN	pmCherry-C1	mCherry:*FKBP1A*(3-108):[GGSA]$_4$GG:PTEN	This study
TagBFP2-FKBP-iSH2	pTagBFP2	TagBFP2:AAAGAGGAA:*FKBP1A*(3-108): [GGSA]$_4$GG:Mus musculus *Pik3r1*(159-349)	(Suh et al., 2006)
NES-EGFP-P4Mx1	pEGFP-C1	*X.leavis map2k1.L*(32-44):EGFP:*L. pneumophila SidM*(546-647)	(Zewe et al., 2018)
PH-PLCD1-EGFP	pEGFP-N1	PLCD1v2(1:170):EGFP	(Várnai and Balla, 1998)
PH-AKT-EGFP	pEGFP-N1	AKT(1-164):EGFP	(Servant et al., 2000)
NES-EGFP-PH-ARNO^{2G}x2	pEGFP-C1	*X.leavis* map2k1.L(32-44):EGFP:CYTH2(252-399):GGSGGVDM: CYTH2(252-399)	This study
NES-EGFP-PH-ARNO$^{2G-I303E}$x2	pEGFP-C1	*X.leavis* map2k1.L(32-44):EGFP:CYTH2(252-399)(I303E):GGSGGVDM: CYTH2(252-399)(I303E)	This study
EGF-FYVE-EEA1	pEGFP-C1	EGFP:EEA1(1253-1411)	(Balla et al., 2000)
pcDNA3-U6H1-X1-HCKRS	pcDNA3	pyrrolysyl-tRNA synthetase/tRNA	(Luo et al., 2014)
TagBFP2-LepB^{K39TAG}-iRFP	pTagBFP2-C1	TagBFP2: *L. pneumophila LepB^{K39TAG}*(1-311):GGSGG:iRFP	This study
mCherry-Rab5	pmCherry-C1	mCherry:*Canis lupus RAB5A*	(Hammond et al., 2014)

Chemicals

Rapamycin (Fisher Scientific BP2963-1) was dissolved in DMSO at 1 mM and stored in aliquots at –20˚C; the final concentration used in cells was 1 μM. 4 mg/ml Insulin zinc solution (ThermoFisher 12585014) was stored in aliquots at –20˚C. GDC-0941 (EMD-Millipore

5.09226.0001) was dissolved in 2 mM DMSO and stored in aliquots at –20˚C. Aliquots of hydroxycoumarin Lysine (Luo et al., 2014) were stored at –20˚C in DMSO at 100 mM.

Microscopy

Cells were imaged in 1.6 ml FluoroBrite DMEM (Life Technologies A1896702) supplemented with 25 mM HEPES (pH 7.4) 1:1000 chemically-defined lipid supplement with or without 10% heat-inactivated fetal bovine serum. For treatments, 0.4 ml of this medium containing 5-fold the final concentration of compound was applied to the dish (or 0.5 ml for a second addition).

Confocal microscopy was performed on a Nikon TiE inverted stand with an A1R resonant scan head and fiber-coupled 4-line excitation LU-NV laser combiner equipped with 405, 488, 561 and 640 nm lines. 8 or 16 frame averages were used to improve signal to noise. A 100x 1.45 NA plan-apochromatic oil-immersion objective was used throughout. Blue (405 nm excitation, 425-475 nm emission) and yellow/orange (561 nm Ex, 570-620 nm Em) channels were imaged concurrently, alternating with concurrent imaging of green (488 nm Ex, 500-550 nm Em), far/infra-red (640 nm Ex, 663-737 nm Em) and a transmitted light channel for DIC. The hexagonal confocal pinhole was set to 1.2x Airy disc size of the longest wavelength imaged.

For TIRFM, we used a second Nikon TiE microscope fitted with a TIRF illuminator arm fiber coupled to an Oxxius L4C laser combined equipped with 405, 488, 561 and 640 nm lasers. A 100x 1.45 NA plan-apochromatic oil-immersion objective was used to deliver the high angle of incidence illuminating beam and acquire the images by epi fluorescence. Images were acquired on a Zyla 5.5 sCMOS camera (Andor) with 2x2 binning in rolling shutter mode. Blue (405 nm) and yellow/orange (561 nm excitation) channels were imaged through a dual pass 420-480 & 570-620 nm filter (Chroma), whereas green (488 nm) and far/infra-red (640 nm excitation) used a dual pass 505-550 & 650-850 nm filter (Chroma).

Optogenetic activation of LepB was performed by confocal microscopy. After acquiring approx. 30 s of data with 405 nm illumination set to zero power, transmission was turned up to 20% of the maximum available power from the LU-NV unit.

For single molecule imaging, PAmCherry was imaged without pixel binning in global shutter mode with 25 ms exposures and 30% illumination power with 561 nm, and 0.8% 405 nm for

photoactivation from the 100 mW Oxxius lasers. A 16x16 μm region of PM was imaged for tracking.

Image Analysis

Images in Nikon nd2 image format were imported into the open access image analysis package Fiji (Schindelin et al.), using the LOCI BioFormats importer (Linkert et al., 2010). A custom written macro was used to combine fields into a single enlarged image for the purposes of image analysis (though never for presentation).

Quantifying the difference in intensities between EGFP and iRFP channels (figure 1B&C): Regions of interest (ROI) were drawn around each cell, and a custom-written macro was used to measure the average pixel intensity in these ROI and then normalize each pixel to this value. The normalized iRFP (cytosolic) image was then subtracted from the normalized EGFP-cPH channel to yield the subtracted image.

Intensity changes in specific compartments imaged by confocal (figures 2B, 4B & C): Cells were measured inside ROI. A second image channel (mCherry-Rab5 in figure 2 and LAMP1-FRB-iRFP in figure 4) was auto-thresholded and used to generate a mask to measure the normalized pixel intensity of the EGFP channel, as previously described in detail (Zewe et al., 2018).

PM Intensity changes imaged by TIRFM (figure 1J-M; figure 3): ROI corresponding to the footprint of individual cells were defined, and after subtracting camera noise, intensity levels over time were measured. Average pixel intensity in each frame t was normalized to the pre-treatment average level F_t/F_{pre}.

Single molecule analysis (figure 1D-H): Single molecule trajectories were segmented and tracked using the open-source Fiji implementation of the "u-track" single particle tracking algorithm (Jaqaman et al., 2008). A "Difference of Gaussians" filter was used with a hard threshold and an estimated dimeter of 0.5 μm for the estimated diameter (i.e. an approx 8x8 pixel neighborhood) of single molecules. Co-ordinates of the trajectories were exported as xml files, and mean-square displacement at different time lags (Vrljic et al., 2007) was calculated along with trajectory lifetime distributions using custom written code in Python.

Selecting representative images for presentation: example images were selected based on having the best signal to noise possible, whilst also having measured values close to the sampled population median, and are always within the central interquartile range.

Data presentation and statistics was performed using Graphpad Prism 7. Data were subject to the D'Agostino and Pearson normality test to select for parametric or non-parametric tests.

Acknowledgements

We thank Vladislav Verkhusha (Albert Einstein College of Medicine) and Tamas Balla (NIH) for generously sharing plasmids. This work was supported by National Institutes of Health grant 1R35GM119412-01 (to G.R.V.H.) and National Science Foundation grant CBET-1603930 (to A.D.)

References

Asano, T., Y. Mochizuki, K. Matsumoto, T. Takenawa, and T. Endo. 1999. Pharbin, a Novel Inositol Polyphosphate 5-Phosphatase, Induces Dendritic Appearances in Fibroblasts. *Biochem Bioph Res Co*. doi:10.1006/bbrc.1999.0998 . 261:188–195.

Bae, Y., Z. Ding, T. Das, A. Wells, F. Gertler, and P. Roy. 2010. Profilin1 regulates PI(3,4)P2 and lamellipodin accumulation at the leading edge thus influencing motility of MDA-MB-231 cells. *Proc National Acad Sci*. doi:10.1073/pnas.1002309107 . 107:21547–21552.

Balla, T., T. Bondeva, and P. Várnai. 2000. How accurately can we image inositol lipids in living cells? *Trends Pharmacol Sci*. doi:10.1016/s0165-6147(00)01500-5 . 21:238–241.

Barnabas, N., and D. Cohen. 2013. Phenotypic and Molecular Characterization of MCF10DCIS and SUM Breast Cancer Cell Lines. *Int J Breast Cancer*. doi:10.1155/2013/872743 . 2013:872743.

Belshaw, P., S. Ho, G. Crabtree, and S. Schreiber. 1996. Controlling protein association and subcellular localization with a synthetic ligand that induces heterodimerization of proteins. *Proc National Acad Sci*. doi:10.1073/pnas.93.10.4604 . 93:4604–4607.

Boucrot, E., A.P. Ferreira, L. Almeida-Souza, S. Debard, Y. Vallis, G. Howard, L. Bertot, N. Sauvonnet, and H.T. McMahon. 2015. Endophilin marks and controls a clathrin-independent endocytic pathway. *Nature*. doi:10.1038/nature14067 . 517:460.

Bui, H.H., P.E. Sanders, D. Bodenmiller, M. Kuo, G.P. Donoho, and A.S. Fischl. 2018. Direct analysis of PI(3,4,5)P3 using liquid chromatography electrospray ionization tandem mass spectrometry. *Anal Biochem*. doi:10.1016/j.ab.2018.02.014 . 547:66–76.

Carpenter, C., B. Duckworth, K. Auger, B. Cohen, B. Schaffhausen, and L. Cantley. 1990. Purification and characterization of phosphoinositide 3-kinase from rat liver. *J Biological Chem*. 265:19704–11.

Coq, J., M. Camacho-Artacho, J. Velázquez, C. ntiveri, L. Gallego, R. Campos-Olivas, N. Dölker, and D. Lietha. 2017. Structural basis for interdomain communication in SHIP2 providing high phosphatase activity. *Elife*. doi:10.7554/elife.26640 . 6:e26640.

Courtney, T., and A. Deiters. 2018. Recent advances in the optical control of protein function through genetic code expansion. *Curr Opin Chem Biol*. doi:10.1016/j.cbpa.2018.07.011 . 46:99–107.

Cronin, T.C., J.P. DiNitto, M.P. Czech, and D.G. Lambright. 2004. Structural determinants of phosphoinositide selectivity in splice variants of Grp1 family PH domains. *Embo J*. doi:10.1038/sj.emboj.7600388 . 23:3711–3720.

Damen, J., L. Liu, P. Rosten, R. Humphries, A. Jefferson, P. Majerus, and G. Krystal. 1996. The 145-kDa protein induced to associate with Shc by multiple cytokines is an inositol tetraphosphate and phosphatidylinositol 3,4,5-triphosphate 5-phosphatase. *Proc National Acad Sci*. doi:10.1073/pnas.93.4.1689 . 93:1689–1693.

Domin, J., F. Pages, S. Volinia, S.E. Rittenhouse, M.J. Zvelebil, R.C. Stein, And M.D. Waterfield. 1997. Cloning of a human phosphoinositide 3-kinase with a C2 domain that displays reduced sensitivity to the inhibitor wortmannin. *Biochem J*. doi:10.1042/bj3260139 . 326:139–147.

Dong, N., M. Niu, L. Hu, Q. Yao, R. Zhou, and F. Shao. 2016. Modulation of membrane phosphoinositide dynamics by the phosphatidylinositide 4-kinase activity of the Legionella LepB effector. *Nat Microbiol*. doi:10.1038/nmicrobiol.2016.236 . 2:nmicrobiol2016236.

Dowler, S., R.A. Currie, D.G. Campbell, M. Deak, G. Kular, P.C. Downes, And D.R. Alessi. 2000. Identification of pleckstrin-homology-domain-containing proteins with novel phosphoinositide-binding specificities. *Biochem J*. doi:10.1042/bj3510019 . 351:19–31.

Ebner, M., I. Lučić, T.A. Leonard, and I. Yudushkin. 2017. PI(3,4,5)P3 Engagement Restricts Akt Activity to Cellular Membranes. *Mol Cell*. doi:10.1016/j.molcel.2016.12.028 . 65:416-431.e6.

Feng, S., V. Laketa, F. Stein, A. Rutkowska, A. MacNamara, S. Depner, U. Klingmüller, J. Saez-Rodriguez, and C. Schultz. 2014. A Rapidly Reversible Chemical Dimerizer System to Study Lipid Signaling in Living Cells. *Angewandte Chemie International Edition*. doi:10.1002/anie.201402294 . 53:6720–6723.

Fruman, D.A., H. Chiu, B.D. Hopkins, S. Bagrodia, L.C. Cantley, and R.T. Abraham. 2017. The PI3K Pathway in Human Disease. *Cell*. doi:10.1016/j.cell.2017.07.029 . 170:605–635.

Fujiwara, T.K., K. Iwasawa, Z. Kalay, T.A. Tsunoyama, Y. Watanabe, Y.M. Umemura, H. Murakoshi, K.G. Suzuki, Y.L. Nemoto, N. Morone, and A. Kusumi. 2016. Confined diffusion of transmembrane proteins and lipids induced by the same actin meshwork lining the plasma membrane. *Mol Biol Cell*. doi:10.1091/mbc.e15-04-0186 . 27:1101–1119.

Furutani, M., K. Tsujita, T. Itoh, T. Ijuin, and T. Takenawa. 2006. Application of phosphoinositide-binding domains for the detection and quantification of specific phosphoinositides. *Analytical Biochemistry*. doi:10.1016/j.ab.2006.05.014 . 355:8–18.

Gewinner, C., Z.C. Wang, A. Richardson, J. Teruya-Feldstein, D. Etemadmoghadam, D. Bowtell, J. Barretina, W.M. Lin, L. Rameh, L. Salmena, P. Pandolfi, and L.C. Cantley. 2009. Evidence that Inositol Polyphosphate 4-Phosphatase Type II Is a Tumor Suppressor that Inhibits PI3K Signaling. *Cancer Cell*. doi:10.1016/j.ccr.2009.06.006 . 16:115–125.

Gray, A., and D.R. Alessi. 2011. Role of TAPP1 and TAPP2 adaptor binding to PtdIns(3,4)P2 in regulating insulin sensitivity defined by knock-in analysis. *The Biochemical journal*. doi:10.1042/BJ20102012 . 434:265–274.

Guilherme, A., J. Klarlund, G. Krystal, and M. Czech. 1996. Regulation of phosphatidylinositol 3,4,5-trisphosphate 5'-phosphatase activity by insulin. *The Journal of biological chemistry*. 271:29533–6.

Hammond, G., M.P. Machner, and T. Balla. 2014. A novel probe for phosphatidylinositol 4-phosphate reveals multiple pools beyond the Golgi. *J Cell Biology*. doi:10.1083/jcb.201312072 . 205:113–126.

Hawkins, P., T. Jackson, and L. Stephens. 1992. Platelet-derived growth factor stimulates synthesis of PtdIns(3,4,5)P3 by activating a PtdIns(4,5)P2 3-OH kinase. *Nature*. doi:10.1038/358157a0 . 358:157–9.

Hawkins, P., and L. Stephens. 2016. Emerging evidence of signalling roles for PI(3,4)P2 in Class I and II PI3K-regulated pathways. *Biochem Soc T*. doi:10.1042/bst20150248 . 44:307–314.

He, K., R. III, gokul Upadhyayula, E. Song, S. Dang, B.R. Capraro, W. Wang, W. Skillern, R. Gaudin, M. Ma, and T. Kirchhausen. 2017. Dynamics of phosphoinositide conversion in clathrin-mediated endocytic traffic. *Nature*. doi:10.1038/nature25146 . 552:410.

Hofmann, I., A. Thompson, C.M. Sanderson, and S. Munro. 2007. The Arl4 Family of Small G Proteins Can Recruit the Cytohesin Arf6 Exchange Factors to the Plasma Membrane. *Current Biology*. doi:10.1016/j.cub.2007.03.007 . 17:711–716.

Hogan, A., Y. Yakubchyk, J. Chabot, C. Obagi, E. Daher, K. Maekawa, and S.H. Gee. 2004. The Phosphoinositol 3,4-Bisphosphate-binding Protein TAPP1 Interacts with Syntrophins and Regulates Actin Cytoskeletal Organization. *Journal of Biological Chemistry*. doi:10.1074/jbc.M410654200 . 279:53717–53724.

Hopkins, B.D., C. Pauli, D. Xing, D.G. Wang, X. Li, D. Wu, S.C. Amadiume, M.D. Goncalves, C. Hodakoski, M.R. Lundquist, R. Bareja, Y. Ma, E.M. Harris, A. Sboner, H. Beltran, M.A. Rubin, S. Mukherjee, and L.C. Cantley. 2018. Suppression of insulin feedback enhances the efficacy of PI3K inhibitors. *Nature*. doi:10.1038/s41586-018-0343-4 . 1–5.

Ishihara, H., T. Sasaoka, H. Hori, T. Wada, H. Hirai, T. Haruta, W.J. Langlois, and M. Kobayashi. 1999. Molecular Cloning of Rat SH2-Containing Inositol Phosphatase 2 (SHIP2) and Its Role in the Regulation of Insulin Signaling. *Biochem Bioph Res Co*. doi:10.1006/bbrc.1999.0888 . 260:265–272.

Jackson, T., L. Stephens, and P. Hawkins. 1992. Receptor specificity of growth factor-stimulated synthesis of 3-

phosphorylated inositol lipids in Swiss 3T3 cells. *J Biological Chem*. 267:16627–36.

Jaqaman, K., D. Loerke, M. Mettlen, H. Kuwata, S. Grinstein, S.L. Schmid, and G. Danuser. 2008. Robust single-particle tracking in live-cell time-lapse sequences. *Nat Methods*. doi:10.1038/nmeth.1237 . 5:nmeth.1237.

Kimber, W.A., L. Trinkle-Mulcahy, P.C. Cheung, M. Deak, L.J. Marsden, A. Kieloch, S. Watt, R.T. Javier, A. Gray, C. Downes, J.M. Lucocq, and D.R. Alessi. 2002. Evidence that the tandem-pleckstrin-homology-domain-containing protein TAPP1 interacts with Ptd(3,4)P2 and the multi-PDZ-domain-containing protein MUPP1 in vivo. *The Biochemical journal*. doi:10.1042/bj3610525 . 361:525–36.

Kong, A.M., C.J. Speed, C.J. O'Malley, M.J. Layton, T. Meehan, K.L. Loveland, S. Cheema, L.M. Ooms, and C.A. Mitchell. 2000. Cloning and characterization of a 72 kDa inositol polyphosphate 5-phosphatase localized to the Golgi. *J Biol Chem*. doi:10.1074/jbc.m000874200 . 275:24052–24064.

Kong, D., S. Dan, K. Yamazaki, and T. Yamori. 2010. Inhibition profiles of phosphatidylinositol 3-kinase inhibitors against PI3K superfamily and human cancer cell line panel JFCR39. *European Journal of Cancer*. doi:10.1016/j.ejca.2010.01.005 . 46:1111–1121.

Krause, M., J.D. Leslie, M. Stewart, E.M. Lafuente, F. Valderrama, R. Jagannathan, G.A. Strasser, D.A. Rubinson, H. Liu, M. Way, M.B. Yaffe, V.A. Boussiotis, and F.B. Gertler. 2004. Lamellipodin, an Ena/VASP Ligand, Is Implicated in the Regulation of Lamellipodial Dynamics. *Dev Cell*. doi:10.1016/j.devcel.2004.07.024 . 7:571–583.

Landego, I., N. Jayachandran, S. Wullschleger, T. Zhang, I.W. Gibson, A. Miller, D.R. Alessi, and A.J. Marshall. 2012. Interaction of TAPP adapter proteins with phosphatidylinositol (3,4)-bisphosphate regulates B-cell activation and autoantibody production. *European Journal of Immunology*. doi:10.1002/eji.201242371 . 42:2760–2770.

Li, H., and A.J. Marshall. 2015. Phosphatidylinositol (3,4) bisphosphate-specific phosphatases and effector proteins: A distinct branch of PI3K signaling. *Cell Signal*. doi:10.1016/j.cellsig.2015.05.013 . 27:1789–1798.

Linkert, M., C.T. Rueden, C. Allan, J.-M.M. Burel, W. Moore, A. Patterson, B. Loranger, J. Moore, C. Neves, D. Macdonald, A. Tarkowska, C. Sticco, E. Hill, M. Rossner, K.W. Eliceiri, and J.R. Swedlow. 2010. Metadata matters: access to image data in the real world. *The Journal of cell biology*. doi:10.1083/jcb.201004104 . 189:777–82.

Liu, J., J. Hemphill, S. Samanta, M. Tsang, and A. Deiters. 2017. Genetic Code Expansion in Zebrafish Embryos and Its Application to Optical Control of Cell Signaling. *J Am Chem Soc*. doi:10.1021/jacs.7b02145 . 139:9100–9103.

Luo, J., R. Uprety, Y. Naro, C. Chou, D.P. Nguyen, J.W. Chin, and A. Deiters. 2014. Genetically Encoded Optochemical Probes for Simultaneous Fluorescence Reporting and Light Activation of Protein Function with Two-Photon Excitation. *Journal of the American Chemical Society*. doi:10.1021/ja5055862 . 136:15551–15558.

Malek, M., A. Kielkowska, T. Chessa, K.E. Anderson, D. Barneda, P. Pir, H. Nakanishi, S. Eguchi, A. Koizumi, J. Sasaki, V. Juvin, V.Y. Kiselev, I. Niewczas, A. Gray, A. Valayer, D. Spensberger, M. Imbert, S. Felisbino, T. Habuchi, S. Beinke, S. Cosulich, N. Novère, T. Sasaki, J. Clark, P.T. Hawkins, and L.R. Stephens. 2017. PTEN Regulates PI(3,4)P2 Signaling Downstream of Class I PI3K. *Mol Cell*. doi:10.1016/j.molcel.2017.09.024 . 68:566-580.e10.

Manley, S., J.M. Gillette, G.H. Patterson, H. Shroff, H.F. Hess, E. Betzig, and J. Lippincott-Schwartz. 2008. High-density mapping of single-molecule trajectories with photoactivated localization microscopy. *Nat Methods*. doi:10.1038/nmeth.1176 . 5:nmeth.1176.

Manna, D., A. Albanese, W. Park, and W. Cho. 2007. Mechanistic Basis of Differential Cellular Responses of Phosphatidylinositol 3,4-Bisphosphate- and Phosphatidylinositol 3,4,5-Trisphosphate-binding Pleckstrin Homology Domains. *J Biol Chem*. doi:10.1074/jbc.m703517200 . 282:32093–32105.

Marat, A.L., A. Wallroth, W.-T. Lo, R. Müller, G. Norata, M. Falasca, C. Schultz, and V. Haucke. 2017. mTORC1 activity repression by late endosomal phosphatidylinositol 3,4-bisphosphate. *Science*. doi:10.1126/science.aaf8310 . 356:968–972.

Marshall, A.J., A.K. Krahn, K. Ma, V. Duronio, and S. Hou. 2002. TAPP1 and TAPP2 Are Targets of Phosphatidylinositol 3-Kinase Signaling in B Cells: Sustained Plasma Membrane Recruitment Triggered by the B-Cell

Antigen Receptor. *Mol Cell Biol*. doi:10.1128/mcb.22.15.5479-5491.2002 . 22:5479–5491.

McConnachie, G., I. Pass, S.M. Walker, and P.C. Downes. 2003. Interfacial kinetic analysis of the tumour suppressor phosphatase, PTEN: evidence for activation by anionic phospholipids. *The Biochemical journal*. doi:10.1042/bj20021848 . 371:947–955.

Naguib, A., G. Bencze, H. Cho, W. Zheng, A. Tocilj, E. Elkayam, C.R. Faehnle, N. Jaber, C.P. Pratt, M. Chen, W.-X. Zong, M.S. Marks, L. Joshua-Tor, D.J. Pappin, and L.C. Trotman. 2015. PTEN Functions by Recruitment to Cytoplasmic Vesicles. *Mol Cell*. doi:10.1016/j.molcel.2015.03.011 . 58:255–268.

Oikawa, T., T. Itoh, and T. Takenawa. 2008. Sequential signals toward podosome formation in NIH-src cells. *J Cell Biology*. doi:10.1083/jcb.200801042 . 182:157–169.

Ong, C.J., A. Ming-Lum, M. Nodwell, A. Ghanipour, L. Yang, D.E. Williams, J. Kim, L. Demirjian, P. Qasimi, J. Ruschmann, L.-P. Cao, K. Ma, S.W. Chung, V. Duronio, R.J. Andersen, G. Krystal, and A. Mui. 2007. Small-molecule agonists of SHIP1 inhibit the phosphoinositide 3-kinase pathway in hematopoietic cells. *Blood*. doi:10.1182/blood-2007-03-079699 . 110:1942–1949.

Pesesse, X., S. Deleu, F. Smedt, L. Drayer, and C. Erneux. 1997. Identification of a Second SH2-Domain-Containing Protein Closely Related to the Phosphatidylinositol Polyphosphate 5-Phosphatase SHIP. *Biochem Bioph Res Co*. doi:10.1006/bbrc.1997.7538 . 239:697–700.

Posor, Y., M. Eichhorn-Gruenig, D. Puchkov, J. Schöneberg, A. Ullrich, A. Lampe, R. Müller, S. Zarbakhsh, F. Gulluni, E. Hirsch, M. Krauss, C. Schultz, J. Schmoranzer, F. Noé, and V. Haucke. 2013. Spatiotemporal control of endocytosis by phosphatidylinositol-3,4-bisphosphate. *Nature*. doi:10.1038/nature12360 . 499:233.

Rosselli-Murai, L.K., J.A. Yates, S. Yoshida, J. Bourg, K.K. Ho, M. White, J. Prisby, X. Tan, M. Altemus, L. Bao, Z.-F. Wu, S.L. Veatch, J.A. Swanson, S.D. Merajver, and A.P. Liu. 2018. Loss of PTEN promotes formation of signaling-capable clathrin-coated pits. *J Cell Sci*. doi:10.1242/jcs.208926 . 131:jcs208926.

Schindelin, J., I. Arganda-Carreras, E. Frise, V. Kaynig, M. Longair, T. Pietzsch, S. Preibisch, C. Rueden, S. Saalfeld, B. Schmid, J.-Y. Tinevez, D. White, V. Hartenstein, K. Eliceiri, P. Tomancak, and A. Cardona. Fiji: an open-source platform for biological-image analysis. *Nature Methods*. doi:10.1038/nmeth.2019 . 9:676–682.

Schöneberg, J., M. Lehmann, A. Ullrich, Y. Posor, W.-T. Lo, G. Lichtner, J. Schmoranzer, V. Haucke, and F. Noé. 2017. Lipid-mediated PX-BAR domain recruitment couples local membrane constriction to endocytic vesicle fission. *Nat Commun*. doi:10.1038/ncomms15873 . 8:ncomms15873.

Servant, G., O.D. Weiner, P. Herzmark, T. Balla, J.W. Sedat, and H.R. Bourne. 2000. Polarization of Chemoattractant Receptor Signaling During Neutrophil Chemotaxis. *Science*. doi:10.1126/science.287.5455.1037 . 287:1037–1040.

Sharma, V.P., R. Eddy, D. Entenberg, M. Kai, F.B. Gertler, and J. Condeelis. 2013. Tks5 and SHIP2 Regulate Invadopodium Maturation, but Not Initiation, in Breast Carcinoma Cells. *Current Biology*. doi:10.1016/j.cub.2013.08.044 . 23:2079–2089.

Shin, H.-W., M. Hayashi, S. Christoforidis, S. Lacas-Gervais, S. Hoepfner, M.R. Wenk, J. Modregger, S. Uttenweiler-Joseph, M. Wilm, A. Nystuen, W.N. Frankel, M. Solimena, P. Camilli, and M. Zerial. 2005. An enzymatic cascade of Rab5 effectors regulates phosphoinositide turnover in the endocytic pathway. *J Cell Biology*. doi:10.1083/jcb.200505128 . 170:607–618.

Stephens, L., K. Hughes, and R. Irvine. 1991. Pathway of phosphatidylinositol(3,4,5)-trisphosphate synthesis in activated neutrophils. *Nature*. doi:10.1038/351033a0 . 351:33–39.

Subach, F.V., G.H. Patterson, S. Manley, J.M. Gillette, J. Lippincott-Schwartz, and V.V. Verkhusha. 2009. Photoactivatable mCherry for high-resolution two-color fluorescence microscopy. *Nat Methods*. doi:10.1038/nmeth.1298 . 6:nmeth.1298.

Suh, B.-C., T. Inoue, T. Meyer, and B. Hille. 2006. Rapid Chemically Induced Changes of PtdIns(4,5)P_2 Gate KCNQ Ion Channels. *Science*. doi:10.1126/science.1131163 . 314:1454–1457.

Teruel, M.N., and T. Meyer. 2000. Translocation and Reversible Localization of Signaling Proteins A Dynamic Future for Signal Transduction. *Cell*. doi:10.1016/s0092-8674(00)00109-4 . 103:181–184.

Thalappilly, S., M. Suliman, O. Gayet, P. Soubeyran, A. Hermant, P. Lecine, J.L. Iovanna, and N.J. Dusetti. 2008. Identification of multi-SH3 domain-containing protein interactome in pancreatic cancer: A yeast two-hybrid approach. *PROTEOMICS*. doi:10.1002/pmic.200701157 . 8:3071–3081.

Thomas, C.C., S. Dowler, M. Deak, D.R. Alessi, And D. Van Aalten. 2001. Crystal structure of the phosphatidylinositol 3,4-bisphosphate-binding pleckstrin homology (PH) domain of tandem PH-domain-containing protein 1 (TAPP1): molecular basis of lipid specificity. *Biochem J*. doi:10.1042/bj3580287 . 358:287–294.

Trésaugues, L., C. Silvander, S. Flodin, M. Welin, T. Nyman, S. Gräslund, M. Hammarström, H. Berglund, and P. Nordlund. 2014. Structural Basis for Phosphoinositide Substrate Recognition, Catalysis, and Membrane Interactions in Human Inositol Polyphosphate 5-Phosphatases. *Structure*. doi:10.1016/j.str.2014.01.013 . 22:744–755.

Vanhaesebroeck, B., L. Stephens, and P. Hawkins. 2012. PI3K signalling: the path to discovery and understanding. *Nat Rev Mol Cell Bio*. doi:10.1038/nrm3290 . 13:nrm3290.

Várnai, P., and T. Balla. 1998. Visualization of Phosphoinositides That Bind Pleckstrin Homology Domains: Calcium- and Agonist-induced Dynamic Changes and Relationship to Myo-[3H]inositol-labeled Phosphoinositide Pools. *J Cell Biology*. doi:10.1083/jcb.143.2.501 . 143:501–510.

Venkateswarlu, K., P.B. Oatey, J.M. Tavaré, and P.J. Cullen. 1998. Insulin-dependent translocation of ARNO to the plasma membrane of adipocytes requires phosphatidylinositol 3-kinase. *Curr Biol*. doi:10.1016/s0960-9822(98)70181-2 . 8:463–466.

Vrljic, M., S.Y. Nishimura, and W. Moerner. 2007. Single-molecule tracking. *Springer*. 193–219.

Wang, H., W.-T. Lo, A. Žagar, F. Gulluni, M. Lehmann, L. Scapozza, V. Haucke, and O. Vadas. 2018. Autoregulation of Class II Alpha PI3K Activity by Its Lipid-Binding PX-C2 Domain Module. *Molecular Cell*. doi:10.1016/j.molcel.2018.06.042 . 71:343-351.e4.

Watton, S.J., and J. Downward. 1999. Akt/PKB localisation and 3′ phosphoinositide generation at sites of epithelial cell–matrix and cell–cell interaction. *Curr Biol*. doi:10.1016/s0960-9822(99)80192-4 . 9:433–436.

Wills, R.C., B.D. Goulden, and G.R. Hammond. 2018. Genetically encoded lipid biosensors. *Molecular Biology of the Cell*. doi:10.1091/mbc.e17-12-0738 . 29:1526–1532.

Zewe, J.P., R.C. Wills, S. Sangappa, B.D. Goulden, and G.R. Hammond. 2018. SAC1 degrades its lipid substrate PtdIns4P in the endoplasmic reticulum to maintain a steep chemical gradient with donor membranes. *eLife*. doi:10.7554/eLife.35588 . 7:e35588.

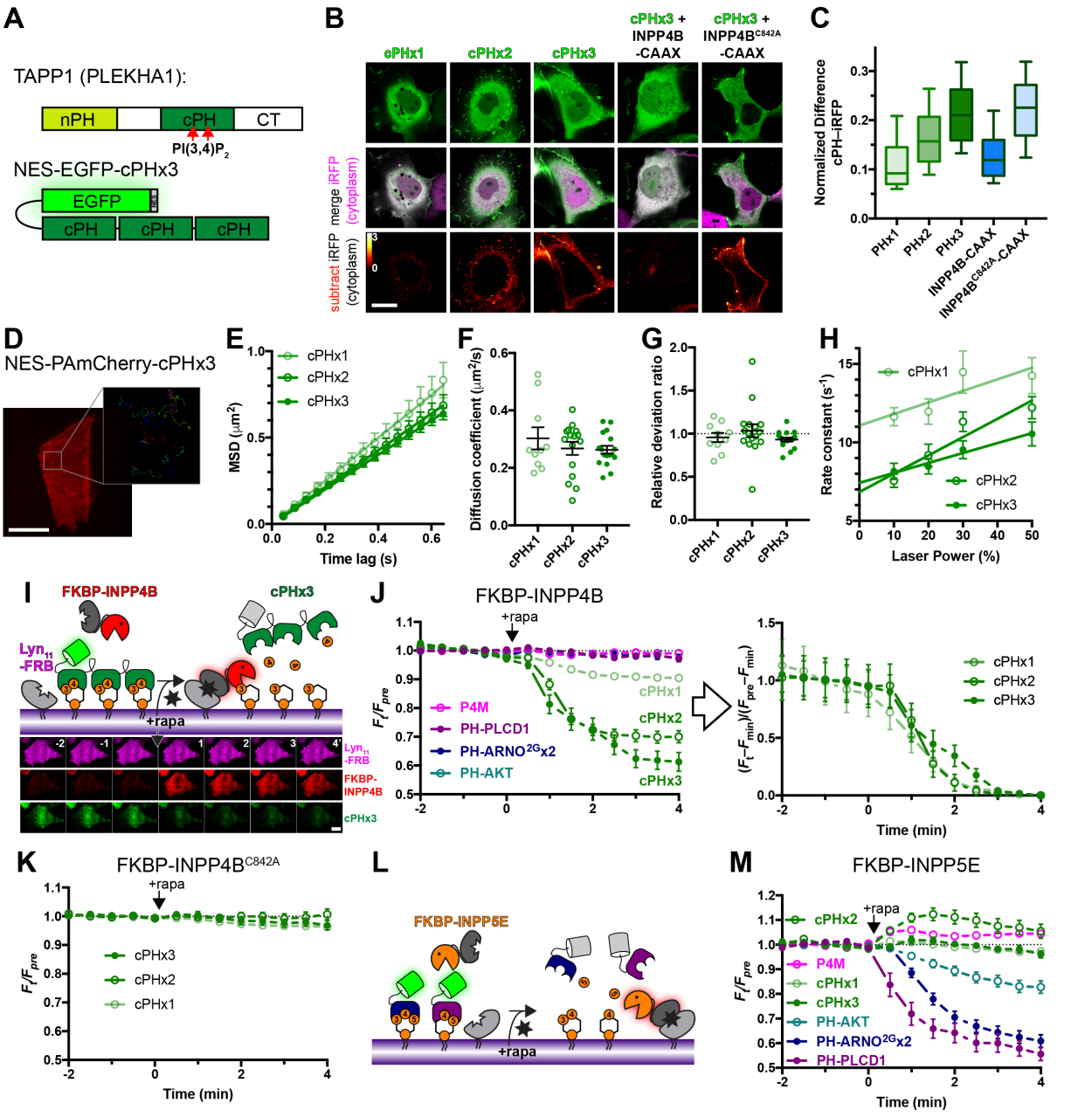

Figure 1: TAPP1 cPHx3 binds PM PI(3,4)P_2 selectively. (**A**) domain structure of full-length TAPP1 protein, along with the EGFP-tandem cPHx3 fusion incorporating a nuclear export sequence (NES). (**B-C**) **cPHx2 and cPHx3 bind the PM in a PI(3,4)P_2-dependent manner in COS-7 grown in 10% serum**. Confocal sections (B) are shown of cells expressing EGFP-cPH plasmids and iRFP to mark the cytoplasm. Subtracting normalized iRFP signal from normalized EGFP reveals PM localization of cPHx2 and cPHx3, which is removed by co-expressing CAAX-box tagged PI(3,4)P_2-phosphatase INPP4B, but not its inactive mutant C842A. Scale bar = 20 μm. The box and whisker plots show median, IQR and 10th-90th percentiles of 90-93 cells from three independent experiments. (**D-H**) **Rapid Brownian diffusion of cPH probes**. Image shows COS-7 cell expressing PAmCherry-cPHx3 after photoactivation in TIRF. The inset shows prior trajectories of individual molecules activated at low efficiency, imaged at 16.7 Hz. Scale bar = 20 μm (2 μm for inset). (E) shows mean square displacement vs time lag plots for indicated cPH probes; data are grand means with s.e.m. of 10 (cPHx1), 16 (cPHx2) or 17 (cPHx3) cells. Individual mean cellular diffusion coefficients (F), relative deviation ratio from Brownian motion (G) and "off rate" constant of trajectory lifetimes (from one-phase exponential fit at each laser power, 10-11 cells) are shown with means ± s.e.m. (**I-K**) **Acute PI(3,4)P_2 depletion removes cPH probes from the PM**. Chemically-induced dimerization (CID) between FKBP and FRB to

recruit INPP4B to the PM (I); montage shows TIRF images of a representative COS-7 cell, scale bar = 20 μm. The graphs (J) show normalized fluorescence intensity in TIRF of cells expressing Lyn_{11}-FRB-iRFP, mCherry-FKBP-INPP4B and the indicated EGFP-lipid biosensor. Data are means ± s.e.m. of 28-30 cells from three independent experiments. The graph at right is the same data normalized to the maximum change in fluorescence for each cPH construct, to emphasize similar dissociation kinetics. The graph in (K) shows the same experiment for cells expressing a catalytically inactive INPP4B; data are means ± s.e.m. of 27-30 cells from three independent experiments. (**L-M**) **PIP_3 or $PI(4,5)P_2$ depletion does not deplete cPH from the PM**. The same experiment as in (I) is depicted, except 5-phopshatase FKBP-INPP5E replaces INPP4B. The graph in (M) shows mean ± s.e.m. of 28-30 cells from three independent experiments.

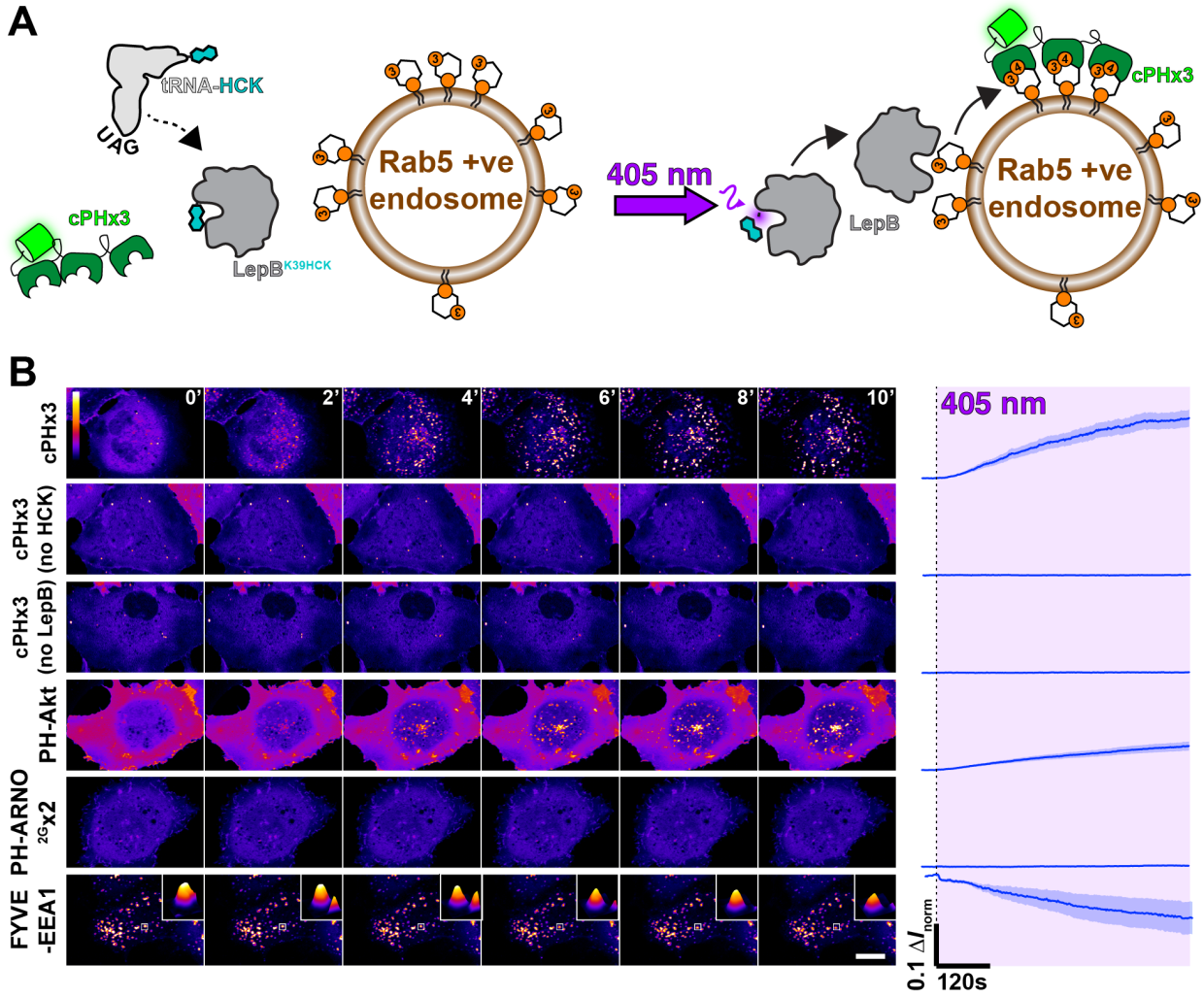

Figure 2: $PI(3,4)P_2$ is sufficient to recruit cPHx3. (**A**) **optogenetic activation of PI3P 4-kinase LepB**. Cells are transfected with a plasmid encoding Amber stop codon (UAG) recognizing tRNA and a tRNA synthase incorporating hydroxycumarin lysine (HCK), along with a LepB mutant containing a K39 to UAG mutation, causing incorporation of active-site blocking HCK into the protein. Upon illumination with 405 nm light, the hydroxycumarin is photolyzed, yielding wild-type K39 and inducing $PI(3,4)P_2$ synthesis on PI3P-replete endosomes. (**B**) **LepB-synthesis of $PI(3,4)P_2$ on endosomes recruits cPHx3 and PH-Akt**, but not the PIP_3 biosensor PH-ARNO^{2G}x2. Images show confocal sections of COS-7 cells transfected with the indicated EGFP-tagged biosensor and the components described in (A) and grown in the presence of HCK. Scale bar = 20 μm. Two controls are shown where either HCK or LepB plasmids were omitted. The graph shows the change in normalized fluorescence intensity in a mask derived from Rab5 puncta (not shown); Trace lines represents mean and shaded area is s.e.m. of 19 (cPHx3), 18 (PH-Akt) or 17 (FYVE and PH-ARNO^{2G}x2) cells from four independent experiments or 5 cells (No HCK or no LepB) from a single experiment.

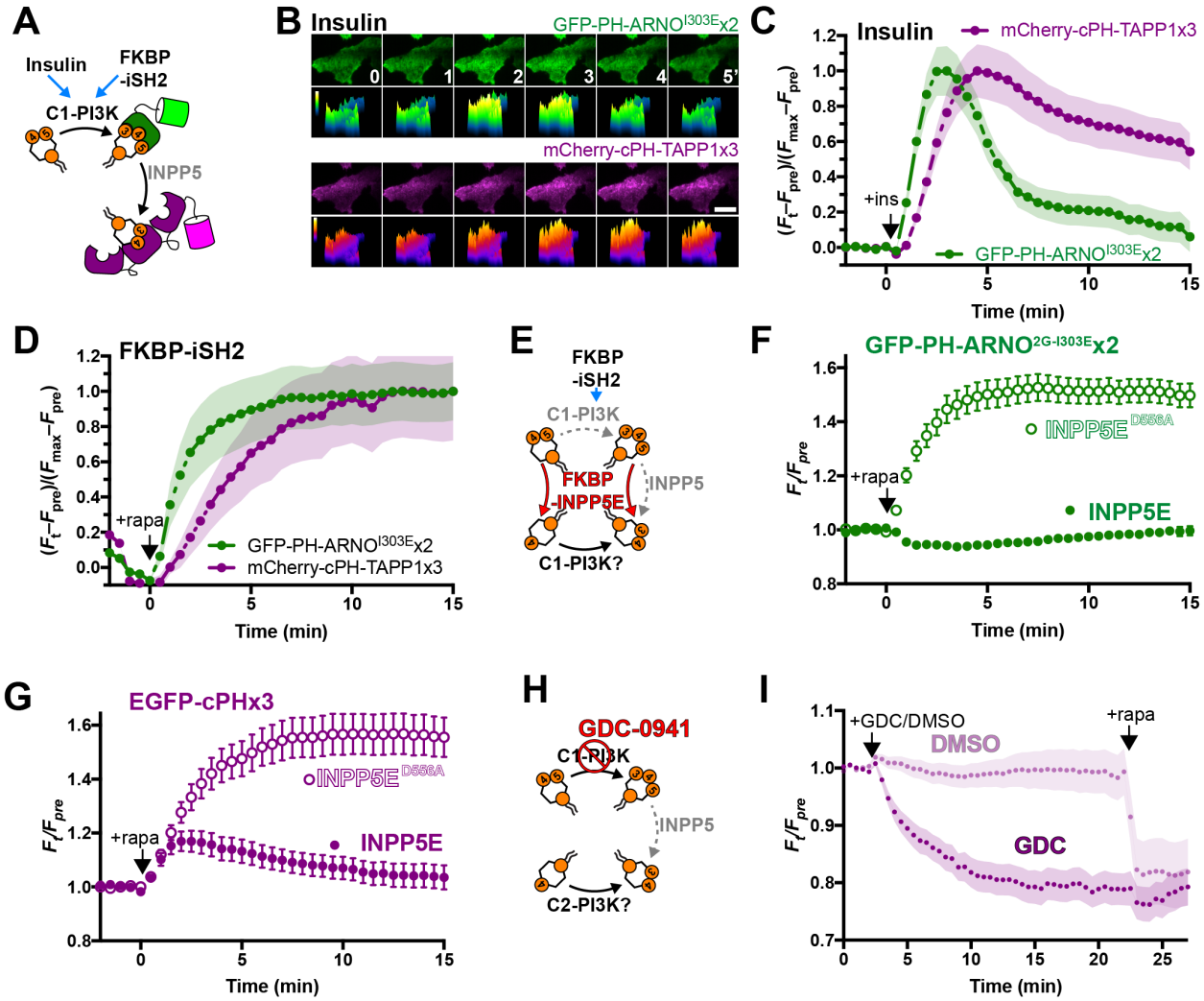

Figure 3: PM PI(3,4)P_2 is derived from PIP_3 synthesized via the class I PI3K pathway. (**A**) activation of the C1-PI3K pathway via insulin stimulation or recruitment of endogenous p110 class I PI3K subunit via CID-mediated recruitment of FKBP-iSH2. (**B-C**) **Insulin-stimulated transient synthesis of PIP_3 and sustained lagging synthesis of PI(3,4)P_2.** TIRF images of HeLa cells (B) expressing PIP_3 biosensor EGFP-PH-ARNO$^{2G\text{-}I303E}$x2 and PI(3,4)P_2 biosensor mCherry-cPHx3 stimulated after time 0 with 200 nM insulin. Scale bar = 20 μm. The graph (C) shows fluorescence intensity data normalized to minimum and maximum intensities, and are means with s.e.m. shaded for 34 cells from three independent experiments. (**D**) **Artificial activation of class I PI3K with iSH2 also induced lagging synthesis of PI(3,4)P_2.** Data are from COS-7 cells expressing the indicated biosensors, along with Lyn_{11}-FRB-iRFP and TagBFP2-FKBP-iSH2. They are normalized to minimum and maximum intensities, and are means with s.e.m. shaded for 31 cells from three independent experiments. (**E-G**) **PI(3,4)P_2 is derived from PIP_3.** (E) The experimental setup is to activate class I PI3K with FKBP-iSH2 whilst simultaneously recruiting the PIP_3 and PI(4,5)P_2-depleting enzyme FKBP-INPP5E, or catalytically inactive D556A mutant as control. Depletion of the PI3K substrate PI(4,5)P_2 leaves 3-phosphorylation of PI4P as the only route of PI(3,4)P_2 synthesis. Graphs show data from COS-7 cells imaged by TIRF expressing PIP_3 biosensor EGFP-PH-ARNO$^{2G\text{-}I303E}$x2 (F) or PI(3,4)P_2 biosensors cPHx3 (G) along with Lyn_{11}-FRB-iRFP, TagBFP2-FKBP-iSH2 and mCherry-FKBP-INPP5E wild-type or D556A, as indicated. Data are means ± s.e.m. of 32-40 cells from three independent experiments. (**H-I**) **Most PI(3,4)P_2 is derived from class I PI3K**. (H) The specific inhibitor GDC-0941 can distinguish class I from class II PI3K activity that could directly produce PI(3,4)P_2. The graph (I) shows normalized fluorescence intensity EGFP-cPHx3 in cells co-transfected with Lyn_{11}-FRB-iRFP and mCherry-FKBP-INPP4B, with CID induced at 22 min to deplete remaining PI(3,4)P_2. 250 nM GDC-0941 or DMSO was added at 2 min. Data are means with s.e.m. shaded for 34 cells from four independent experiments (GDC) or 18 cells from two independent experiments (DMSO).

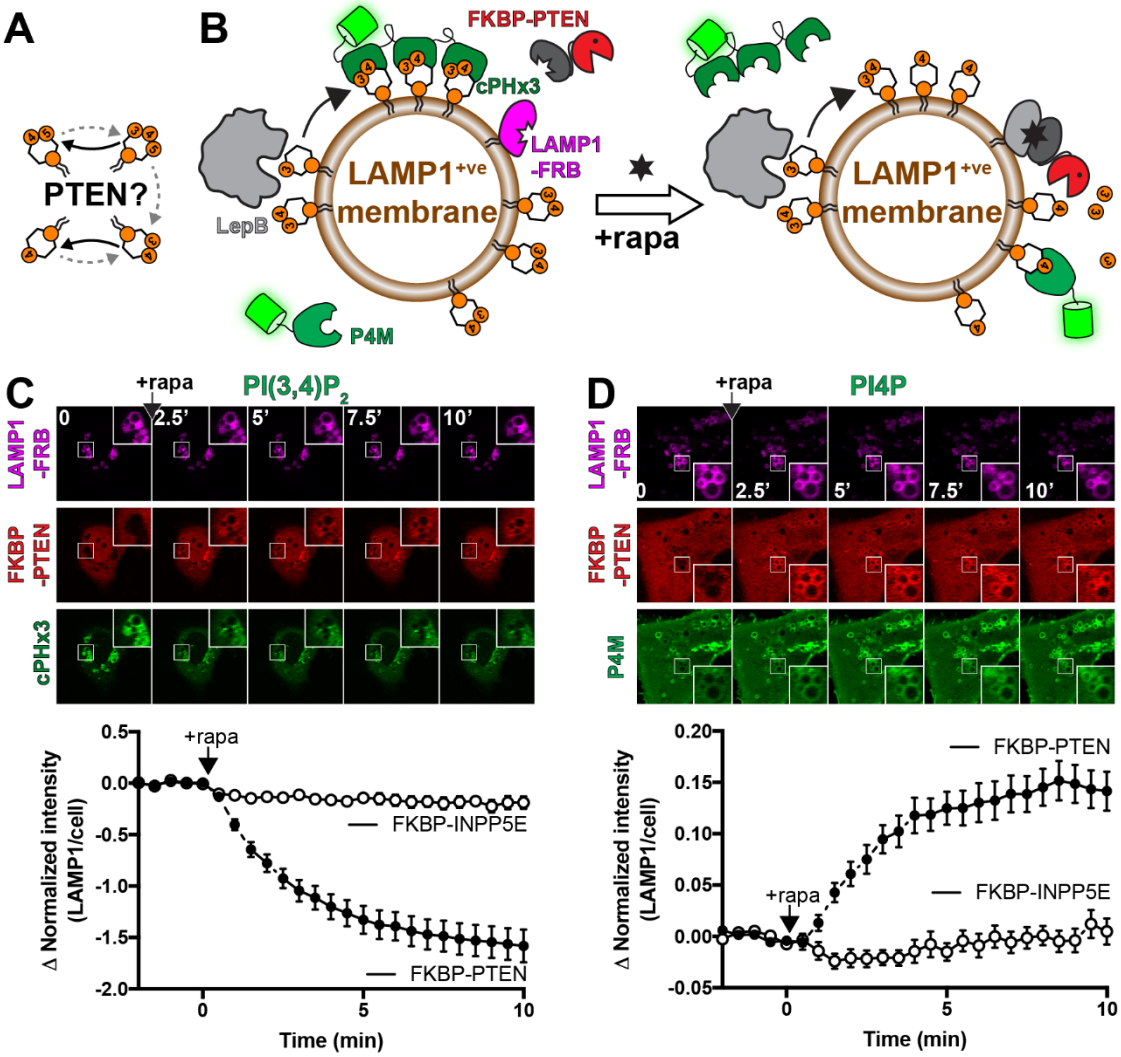

Figure 4: PTEN directly dephosphorylates PI(3,4)P₂. (**A**) Potential PTEN-driven reactions. (**B**) **Experimental setup**. COS-7 cells are expressing active LepB to drive PI(3,4)P_2 in the endosomal system, including (but not limited to) LAMP1-positive membranes. LAMP1-FRB is then used for CID-mediated recruitment of mCherry-FKBP-PTEN to the membranes, where changes in lipids are detected with the indicated biosensors. (**C-D**) **PTEN-mediated conversion of PI(3,4)P₂ to PI4P**. Images show confocal sections of COS-7 cells expressing the indicated constructs before and at the indicated times after CID with rapa. Insets are 5 μm. Data in the graphs are means ± s.e.m. of 32-37 cells from three independent experiments. FKBP-INPP5E serves as a negative control.